Phononic Weyl Nodal Lines and Weyl Pairs in van der Waals Heavy Fermion Material CeSiI

Fulei Li(李复磊)[1,2], Tianye Yu(于天野)[2*], Junwen Lai(赖俊文)[2], Jiaxi Liu(刘嘉希)[2], Peitao Liu(刘培涛)[2], Xing-Qiu Chen(陈星秋)[2*], and Yan Sun(孙岩)[2*]

[1]*School of Materials Science and Engineering, Northeastern University, Shenyang 110819, China*
[2]*Shenyang National Laboratory for Materials Science, Institute of Metal Research, Chinese Academy of Sciences, Shenyang 110016, China*

(Received 11 July 2024; accepted manuscript online 24 September 2024)

Topological phonon is a new frontier in the field of topological materials. Different from electronic structures, phonons are bosons and most topological phonons are metallic form. Previous studies about topological phonon states were focused on three-dimensional (3D) materials. Owing to the lack of material candidates, two-dimensional (2D) and van der Waals f-electron-related topological phonons were rarely reported. Based on first-principles calculations, we investigate the topological phononic state in the heavy fermion material CeSiI with a layered structure. Both 3D bulk and 2D monolayers have topological nontrivial states in the rarely seen f electron dominated van der Waals metal. Owing to the PT and C_{3z} symmetries, Weyl nodal lines with nonzero Chern numbers exist on the hinge of the Brillouin zone. Protected by C_{3z} rotation symmetry, three pairs of Weyl points with $\pm\pi$ Berry phase exist at point K near the frequency of 8 and 10 THz. In addition to the bulk topological charges, corresponding surface/edge states are also systematically analyzed, which gives a consistent understanding. Our results propose another interesting point in the newly discovered rear earth heavy fermion material CeSiI and are helpful for future experimental research of CeSiI topological phonons.

DOI: 10.1088/0256-307X/41/10/107301

In the field of condensed matter physics and materials science, the study of quantum states of matter[1–3] is an important method for exploring the properties of materials. Through theoretical research, many kinds of topological materials[4–7] have been proposed, including topological insulators,[8–11] Dirac/Weyl semimetals,[12–16] and nodal line semimetals,[17–20] some of which have been experimentally confirmed. The electronic topological properties of most materials are related to the symmetry of their crystal structures.[21] Additionally, magnetic materials can exhibit very unique topological phases.[22] Besides the extensive research on topological concepts in electronic systems, topological phonons[23–30] have gradually attracted widespread attention. Unlike electrons, phonons are bosons, representing the collective vibrations of atoms in a crystal. Thus, they are not constrained by the Pauli exclusion principle. Moreover, phonons do not have the concept of a Fermi level and can be physically detected across the entire terahertz phonon spectrum. Phonons are also related to the thermal properties of materials,[31] and their interactions with other particles can induce remarkable and extraordinary effects, such as superconductivity and superfluidity.[32] Through phonons, we can also study the phase transitions and stability of crystal structures.[33,34] Similar to electrons, topological phonons can also generate edge phonon states or topological surface states, which have potential applications in phononic circuits.[35] For example, unidirectional edge quantum states could be used in phonon diodes.[35] To date, various topological phonon states have been discovered in related studies. These states can be classified based on their dimensionality into three categories: zero-dimensional topological nodes[36–41] (including Dirac/Weyl phonons[42–55]), one-dimensional topological nodal lines[56–59] (such as topological Weyl nodal lines,[60–62] nodal rings,[63–71] etc.), and two-dimensional topological surfaces.[72–76]

In the current stage, research of topological phonons has primarily focused on three-dimensional f-electron-free systems. Since most van der Waals materials do not contain f-electron elements, the reports about 2D or van der Waals rear earth topological phononic materials are very few. Thus, it should be interesting to see whether topological phononic states can exist in rear earth 2D and van der Waals materials. Very recently, experiments have discovered a 2D heavy fermion material CeSiI,[77] which exhibits many interesting properties such as Kondo coupling and quantum phase transitions.[78–83] Therefore, the newly discovered van der Waals heavy fermion material CeSiI provides an ideal platform for the study of topological phononic states in 2D and layered rear earth systems

Computational Details. Based on the first-principles calculations and the finite displacement method (FDM), we optimized the lattice constants and determined the

*Corresponding authors. Email: tyyu@imr.ac.cn; xingqiu.chen@imr.ac.cn; yansunning@outlook.com
© 2024 Chinese Physical Society and IOP Publishing Ltd

phonon dispersion. The density functional theory (DFT) and FDM calculations were carried out using the Vienna *ab initio* simulation package (VASP).[84,85] Owing to the strong correlation from f electrons, we employed a PBE + U strategy using the rotationally invariant formulation to describe the strong Coulomb interaction in Ce 4f electrons, with a U value set to 6 eV.[77] The cutoff energy for the plane wave was 500 eV, and the electronic self-consistent energy convergence criterion and the Hellmann–Feynman force on each atom were set to 10^{-8} eV and -0.004 eV/Å, respectively.

We performed calculations for both the 3D bulk and 2D monolayer of CeSiI, belonging to the space group $P\bar{3}m1$. Since the bulk of CeSiI is a layered intermetallic compound, the vdW interactions were considered via the DFT-D3 method. Its optimized lattice constants are $a = b = 4.11$ Å and $c = 11.51$ Å on a Γ-centered k grid of size $16 \times 16 \times 4$ and the force constants are calculated using a $3 \times 3 \times 1$ supercell of CeSiI. For the monolayer of CeSiI, the optimized lattice constant is $a = b = 4.14$ Å, with the CeSiI monolayer thickness of 8.11 Å, on a Γ-centered k grid of size $16 \times 16 \times 1$ and the force constants are calculated using a $4 \times 4 \times 1$ supercell of CeSiI. In the phonon spectrum of CeSiI, a small imaginary frequency was found near the Γ point, caused by numerical errors. This can be eliminated using the rotational sum rules provided by the Hiphive package.[86] We constructed a tight-binding (TB) model of the phonon Hamiltonian, based on which we calculated the topological charges by using the code of the WannierTools package.[87] The surface/edge states were calculated in an iteration of Green's function method.[88]

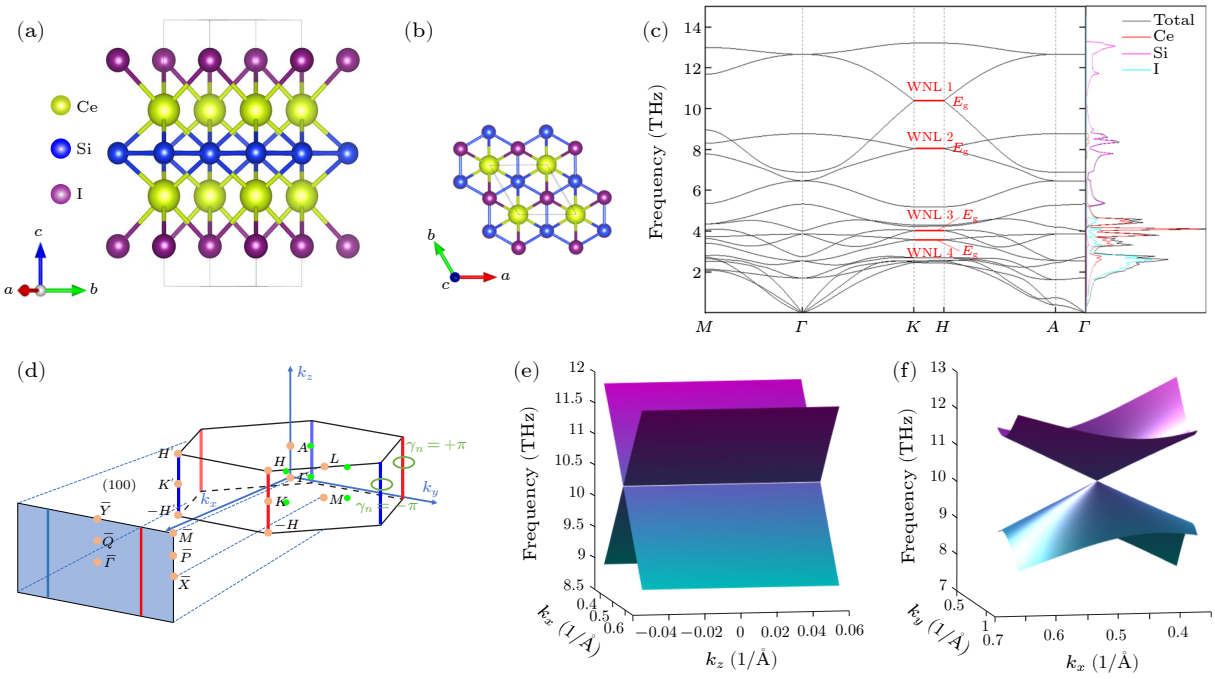

Fig. 1. [(a), (b)] Side and top views of the crystal structure of the bulk of CeSiI. The primitive cell is shown with a solid line. (c) The phonon dispersion of CeSiI along the high-symmetry paths of the Brillouin zone (BZ). Four red thick bands along the K–H path correspond to WNLs with double degeneracy. (d) The bulk BZ and (100) surface BZ of CeSiI. Each WNL traverses the entire BZ along the high-symmetry paths –H–H and –H'–H', where WNL in red (blue) has a positive (negative) Berry phase. (e) The 3D phononic bands around the WNL1 on the $k_y = 0$ plane. (f) The 3D phononic bands around the WNL1 on the $k_z = 0$ plane.

Crystal Structure and Phonon Spectra. The crystal structure is shown in Figs. 1(a) and 1(b). The primitive cell of CeSiI contains 6 atoms, with Ce, Si, and I atoms occupying the 2c (0, 0, 0.16), 2d (0.333, 0.666, 0), and 2d (0.333, 0.666, 0.35) Wyckoff positions, respectively. The phonon dispersion of the bulk of CeSiI along high-symmetry paths is shown in Fig. 1(c). We can see that each branch of phonon dispersion has no imaginary frequencies throughout the entire BZ, illustrating the dynamic stability in the bulk of CeSiI. We also find that there are four WNLs between the high-symmetry points K (0.333, 0.333, 0) and H (0.333, 0.333, 0.5) in the BZ. These Weyl nodal lines are distributed in the BZ. As shown in Fig. 1(d), it is found that these WNLs are perfectly straight along the –H–H path and traverse to the whole BZ. The red (blue) line along –H–H path represents WNL with a positive (negative) Berry phase, and there are three such pairs of WNLs in the whole BZ, indicating that the WNLs are topologically protected by threefold rotational symmetry.

Figures 1(e) and 1(f) present the three-dimensional phonon dispersion diagrams of WNL1 on the $k_y = 0$ and $k_z = 0$ planes, respectively. The phonon dispersion along the $k_z = 0$ plane exhibits linear dispersion, which is characteristic of the Weyl point, as shown in Fig. 1(f). This

means that the four WNLs in Fig. 1(c) are unique for three reasons. Firstly, these WNLs can be regarded as an infinite number of Weyl points densely arranged along the –H–H path. Secondly, these WNLs are precisely located at the boundary of the BZ and traverse the entire BZ along high-symmetry directions. Thirdly, the frequencies of these four WNLs are nearly flat along the –H–H or –H'–H' paths, indicating that they do not vary with the wave vector k, as shown in Fig. 1(c).

Topological Properties of Phonons. To determine the topological nature of these WNLs, we calculated their associated topological invariant of the Berry phase. The Berry phase can be defined by the following formula:

$$\gamma_n = \oint_c A_n(k) \cdot dl, \tag{1}$$

where $A_n(k) = i\langle u_n(k)|\nabla_k|u_n(k)\rangle$ is the Berry connection and $u_n(k)$ is the wave function of the nth band at k. As presented in Fig. 1(c), a close loop centered at a point of WNL on the $k_z = 0$ plane was used to obtain the Berry phase of each WNL. It should be noted that the size of the loop is arbitrary, but it must not encompass other WNLs. Interestingly, we found that the Berry phase of WNL1 and WNL4 along the path –H–H is $+\pi$, while the Berry phase of WNL2 and WNL3 is $-\pi$. This implies that these four WNLs are topologically nontrivial. Additionally, they exhibit the opposite Berry phase along the path –H'–H' compared to the path –H–H due to time reversal symmetry.

Generally, most nodal lines are protected by PT symmetry, while some special symmetries such as rotational and mirror symmetries can restrict nodal lines to high-symmetry paths or mirror planes. We calculated the irreducible representations of each band along the –H–H path. The symmetry of the momentum phonons along this path follows the D_{3d} point group. The irreducible representation states of the four WNLs are E_g, while the other nondegenerate bands are A_{1g} or A_{1u}.

Additionally, these WNLs along the –H–H path remain invariant under the symmetry operation of C_{3z}. Therefore, each state along this path is an eigenstate of C_{3z}, and their eigenvalues are $e^{\pm i2\pi/3}$. The irreducible representations states E_g of C_{3z} correspond to $\begin{pmatrix} e^{i2\pi/3} & 0 \\ 0 & e^{-i2\pi/3} \end{pmatrix}$, which implies that the eigenvalues of two degenerate bands at path –H–H are different eigenvalues. As a result, we can conclude that four WNLs are topologically protected by PT symmetry and C_{3z} symmetry.

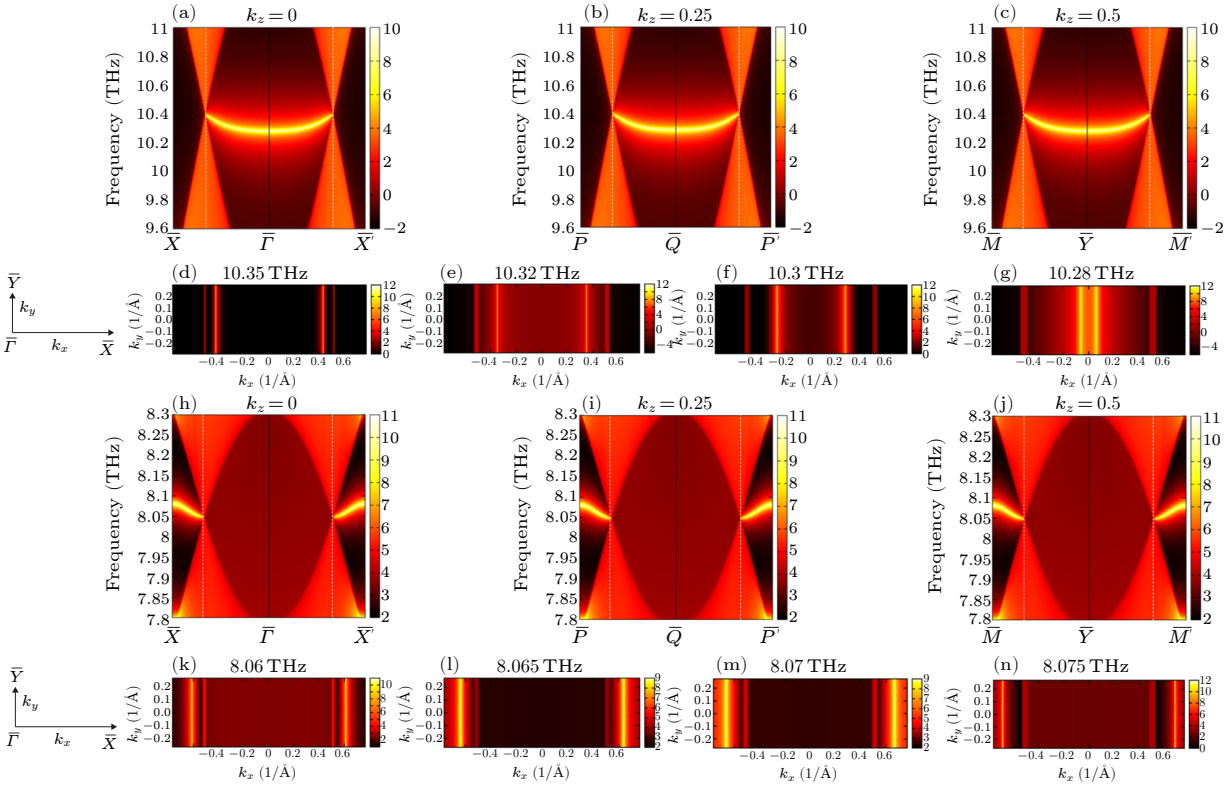

Fig. 2. Surface densities of states and the surface arc states of the (100) surface of CeSiI. (a)–(c) Surface densities of states of WNL1 at different k_z. (d)–(g) The surface arc states around the WNL1 frequency. (h)–(j) Surface densities of states of WNL2 at different k_z. (k)–(n) Surface arc states around the WNL2 frequency.

Phononic Drumhead-Like Surface States. Next, we calculated the surface densities of states of the (100) surface of CeSiI. We only determine the surface states associated with WNL1 and WNL2, while the surface states related to WNL3 and WNL4 are merged into bulk states and cannot be determined. As is expected, the drumhead-like surface states are confined within or outside the rectangle projected on the (100) surface by WNLs along the –H–H and –H'–H' paths. Figure 2 shows the surface states on the CeSiI (100) surface. In Figs. 2(a)–2(c), we have cal-

culated the surface states ranging from 9.6 to 11.0 THz at various k_z values to investigate the topological properties associated with WNL1. Likewise, in Figs. 2(h)–2(j), we have established the surface states with frequency ranging from 7.8 to 8.3 THz to investigate the topological features associated with WNL2, enabling direct comparison with WNL1. Figures 2(a) and 2(h) reveal the presence of bright phonon topologically nontrivial surface states along the high-symmetry path $\overline{X}'$–$\overline{\Gamma}$–$\overline{X}$ on the (100) surface. Furthermore, the surface states originating from the projection point on the path $\overline{X}'$–$\overline{\Gamma}$–$\overline{X}$ of WNL with positive Berry phase and terminate at the projection point of WNL with negative Berry phase are found, illustrating the continuous evolution of surface state characteristics. For both WNL1 and WNL2, their associated surface states are not sensitive to the variation of k_z, consistent with the flatness of WNL1 alone K–H. Additionally, while the surface states associated with WNL1 are confined within the rectangular region projected by WNLs, those related to WNL2 are restricted to an area outside this rectangular region. In Figs. 2(d)–2(g), as the frequency decreases, the WNL1 surface arc states gradually converge towards the central path $\overline{Y}'$–$\overline{\Gamma}$–$\overline{Y}$. However, in Figs. 2(k)–2(n), as the frequency increases, the surface arc states gradually move away from the central path and towards the boundary paths on either side.

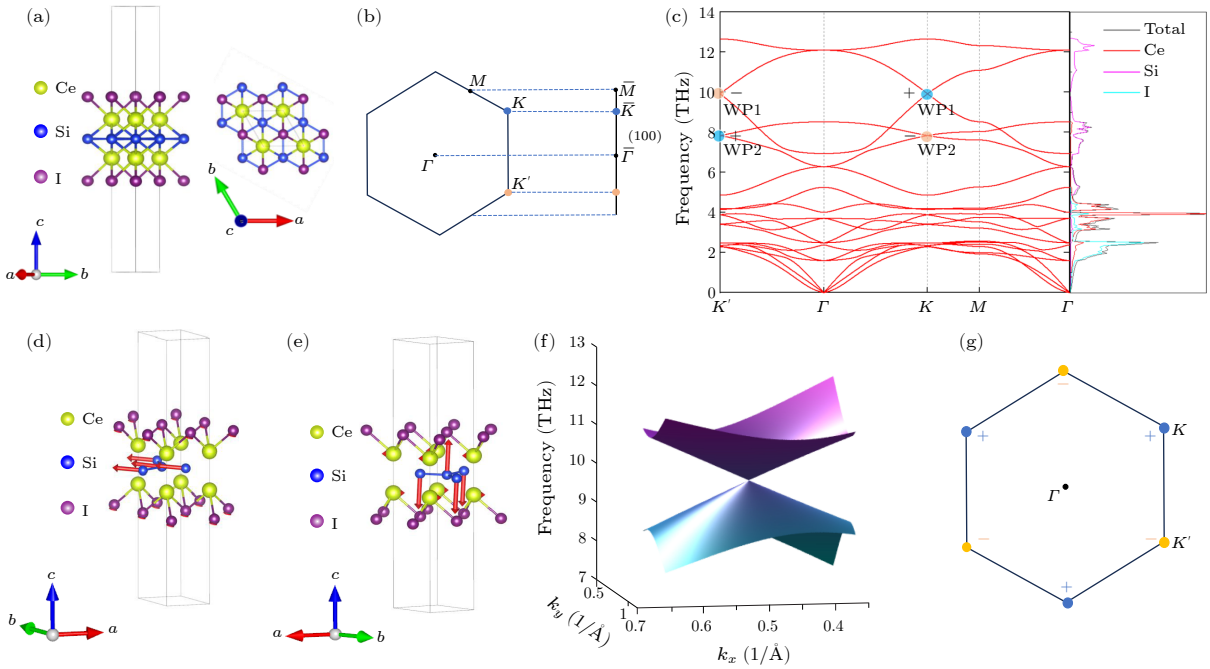

Fig. 3. (a) Side and top views of the crystal structure of the monolayer of CeSiI. The primitive cell is shown with a solid line. (b) Two-dimensional BZ and the (100) edge. (c) Phonon dispersion of the monolayer of CeSiI. [(d), (e)] Three-dimensional visualizations of the atomic vibration modes associated with WP1 and WP2. (f) Three-dimensional phononic bands around the WP1. (g) Distribution of WP1 in the first BZ.

Weyl Pairs Monolayer CeSiI. Lastly, we investigate the phonon topological properties related to the monolayer of CeSiI. Figure 3(a) shows the crystal structure of the monolayer of CeSiI. Figure 3(b) presents its BZ and the (100) edge. The phonon dispersion of the monolayer of CeSiI along the high-symmetry path is shown in Fig. 3(c). It shows that each branch of phonon dispersion has no imaginary frequencies, which proves that the monolayer CeSiI is dynamically stable. We found two phononic Weyl pairs located at the high-symmetry points K and K'. Figures 3(d) and 3(e) show the atomic vibration modes at WP1 and WP2, respectively. WP1 involves the in-plane vibrational mode of Si atoms, and WP2 is mainly determined by the out-of-plane vibrational mode of two Si atoms moving in opposite directions along the c-axis, with a minor contribution from the in-plane vibrational mode of Ce atoms. Figure 3(f) shows the 3D phonon band of WP1, from which it can be seen that WP1 exhibits linear dispersion characteristics.

Berry phase is typically used to characterize the topological charge of Weyl points. The Berry phase of WP1 and WP2 are found to be $+\pi$ and $-\pi$, respectively, as shown in Fig. 3(c). The topological charges of WP1 at K and K' are opposite according to time-reversal symmetry. Three pairs of Weyl points are found in the 2D BZ, which indicates that they are topologically protected by threefold rotational symmetry.

Additionally, we calculated the edge state density of WP1 and WP2, determining the edge states of WP1 and WP2 by adjusting the appropriate frequencies. In Fig. 4(a), a bright edge state connecting one pair of positive and negative WP1 can be found. Similarly, this phe-

nomenon can also be found in WP2. As shown in Fig. 4(b), owing to the existence of a dangling bound-like state, three edge bands are crossing at the projected Weyl point, but two of them have opposite velocities.

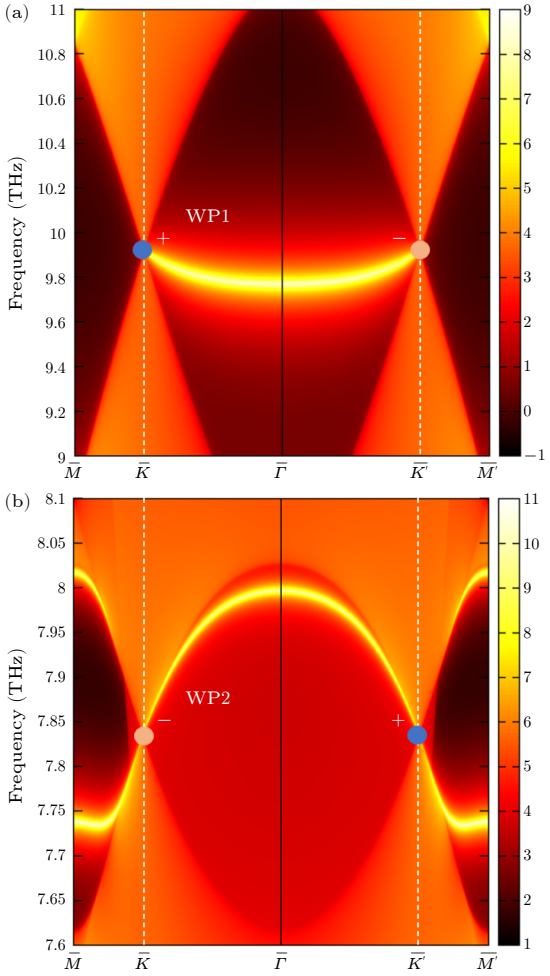

Fig. 4. Edge state density of CeSiI at the (100) edge. [(a), (b)] Edge state densities of WP1 and WP2.

In summary, the topological phonons of CeSiI in both 3D bulk and 2D monolayer are investigated. Four Weyl nodal lines (WNLs) along the high-symmetry path –H–H are found in bulk CeSiI, and they are topologically protected by PT symmetry and C_{3z} symmetry. Calculations of surface densities of states show the presence of the drumhead-like surface states of WNL1 and WNL2, which are located inside and outside the rectangular area projected by the WNLs on the surface. By adjusting their frequencies, we find that as the frequency decreases, the surface arc state of WNL1 gradually moves towards the middle path $\overline{Y}'$–$\overline{\Gamma}$–$\overline{Y}$, while WNL2 behaves oppositely. As for monolayer CeSiI, there are two Weyl points (WP1 and WP2) with opposite Berry phases at the K and K' due to time-reversal symmetry. The edge states always connect pairs of positive and negative Weyl points. This work reveals the rich topological surface and edge states of new discovered rear earth heavy fermion material CeSiI and they are helpful for future experimental understanding of topological phonons.

Acknowledgements. This work was supported by the National Key R&D Program of China (Grant No. 2021YFB3501503), the National Natural Science Foundation of China (Grant Nos. 52271016 and 52188101), and Liaoning Province (Grant No. XLYC2203080). Part of the numerical calculations in this study were carried out on the ORISE Supercomputer (Grant No. DFZX202319).

References

[1] Kosterlitz J M 2017 *Rev. Mod. Phys.* **89** 040501
[2] Chiu C K, Teo J C Y, Schnyder A P, and Ryu S 2016 *Rev. Mod. Phys.* **88** 035005
[3] Goldman N, Budich J C, and Zoller P 2016 *Nat. Phys.* **12** 639
[4] Bradlyn B, Elcoro L, Cano J, Vergniory M G, Wang Z J, Felser C, Aroyo M I, and Bernevig B A 2017 *Nature* **547** 298
[5] Zhang T T, Jiang Y, Song Z D, Huang H, He Y Q, Fang Z, Weng H M, and Fang C 2019 *Nature* **566** 475
[6] Vergniory M G, Elcoro L, Felser C, Regnault N, Bernevig B A, and Wang Z J 2019 *Nature* **566** 480
[7] Tang F, Po H C, Vishwanath A, and Wan X G 2019 *Nature* **566** 486
[8] Konig M, Wiedmann S, Brune C, Roth A, Buhmann H, Molenkamp L W, Qi X L, and Zhang S C 2007 *Science* **318** 766
[9] Hsieh D, Qian D, Wray L, Xia Y, Hor Y S, Cava R J, and Hasan M Z 2008 *Nature* **452** 970
[10] Xia Y, Qian D, Hsieh D, Wray L, Pal A, Lin H, Bansil A, Grauer D, Hor Y S, Cava R J, and Hasan M Z 2009 *Nat. Phys.* **5** 398
[11] Slager R J, Mesaros A, Juričić V, and Zaanen J 2013 *Nat. Phys.* **9** 98
[12] Young S M, Zaheer S, Teo J C Y, Kane C L, Mele E J, and Rappe A M 2012 *Phys. Rev. Lett.* **108** 140405
[13] Wang Z J, Sun Y, Chen X Q, Franchini C, Xu G, Weng H M, Dai X, and Fang Z 2012 *Phys. Rev. B* **85** 195320
[14] Wan X G, Turner A M, Vishwanath A, and Savrasov S Y 2011 *Phys. Rev. B* **83** 205101
[15] Weng H M, Fang C, Fang Z, Bernevig B A, and Dai X 2015 *Phys. Rev. X* **5** 011029
[16] Huang S M, Xu S Y, Belopolski I, Lee C C, Chang G Q, Wang B K, Alidoust N, Bian G, Neupane M, Zhang C L, Jia S, Bansil A, Lin H, and Hasan M Z 2015 *Nat. Commun.* **6** 7373
[17] Li R H, Ma H, Cheng X Y, Wang S L, Li D Z, Zhang Z Y, Li Y Y, and Chen X Q 2016 *Phys. Rev. Lett.* **117** 096401
[18] Schoop L M, Ali M N, Straßer C, Topp A, Varykhalov A, Marchenko D, Duppel V, Parkin S S P, Lotsch B V, and Ast C R 2016 *Nat. Commun.* **7** 11696
[19] Bian G, Chang T R, Sankar R *et al.* 2016 *Nat. Commun.* **7** 10556
[20] Li R, Li J, Wang L, Liu J, Ma H, Song H F, Li D, Li Y, and Chen X Q 2019 *Phys. Rev. Lett.* **123** 136802
[21] Chun Po H, Vishwanath A, and Watanabe H 2017 *Nat. Commun.* **8** 50
[22] Xu Y F, Elcoro L, Song Z D, Wieder B J, Vergniory M G, Regnault N, Chen Y L, Felser C, and Bernevig B A 2020 *Nature* **586** 702
[23] Mousavi S H, Khanikaev A B, and Wang Z 2015 *Nat. Commun.* **6** 8682
[24] He C, Ni X, Ge H, Sun X C, Chen Y B, Lu M H, Liu X P, and Chen Y F 2016 *Nat. Phys.* **12** 1124
[25] Zheng F and Zhang P 2017 *Comput. Phys. Commun.* **210** 139

[26] Lu L, Fu L, Joannopoulos J D, and Soljačić M 2013 *Nat. Photon.* **7** 294
[27] Liu Y Z, Xu Y, and Duan W H 2018 *Natl. Sci. Rev.* **5** 314
[28] Zhang L and Niu Q 2015 *Phys. Rev. Lett.* **115** 115502
[29] Li J, Liu J, Baronett S A, Liu M, Wang L, Li R, Chen Y, Li D, Zhu Q, and Chen X Q 2021 *Nat. Commun.* **12** 1204
[30] Xu Y F, Vergniory M G, Ma D S, Mañes J L, Song Z D, Bernevig B A, Regnault N, and Elcoro L 2024 *Science* **384** eadf8458
[31] Li M L, Shakoori M A, Wang R P, and Li H P 2024 *Chin. Phys. Lett.* **41** 016302
[32] Bardeen J, Cooper L N, and Schrieffer J R 1957 *Phys. Rev.* **108** 1175
[33] Zhang F and Yin L 2022 *Chin. Phys. Lett.* **39** 060301
[34] Liu H, Yu T X, Zhang Z H, and Ying T P 2024 *Chin. Phys. Lett.* **41** 077401
[35] Liu Y Z, Xu Y, Zhang S C, and Duan W H 2017 *Phys. Rev. B* **96** 064106
[36] Wang J, Yuan H, Kuang M, Yang T, Yu Z M, Zhang Z, and Wang X 2021 *Phys. Rev. B* **104** L041107
[37] Xie C, Liu Y, Zhang Z, Zhou F, Yang T, Kuang M, Wang X, and Zhang G 2021 *Phys. Rev. B* **104** 045148
[38] Yang T, Xie C, Chen H, Wang X, and Zhang G 2022 *Phys. Rev. B* **105** 094310
[39] Zhong M, Liu Y, Zhou F, Kuang M, Yang T, Wang X, and Zhang G 2021 *Phys. Rev. B* **104** 085118
[40] Yu W W, Liu Y, Tian L, He T, Zhang X, and Liu G 2022 *J. Phys.: Condens. Matter.* **34** 155703
[41] Liu G, Huang Z, Chen Z, Jin Y, He C, and Xu H 2022 *Phys. Rev. B* **106** 054306
[42] Li J, Xie Q, Ullah S, Li R, Ma H, Li D, Li Y, and Chen X Q 2018 *Phys. Rev. B* **97** 054305
[43] Xie Q, Li J, Ullah S, Li R, Wang L, Li D, Li Y, Yunoki S, and Chen X Q 2019 *Phys. Rev. B* **99** 174306
[44] Zhang T, Song Z, Alexandradinata A, Weng H, Fang C, Lu L, and Fang Z 2018 *Phys. Rev. Lett.* **120** 016401
[45] Miao H, Zhang T T, Wang L, Meyers D, Said A H, Wang Y L, Shi Y G, Weng H M, Fang Z, and Dean M P M 2018 *Phys. Rev. Lett.* **121** 035302
[46] Ding G, Zhou F, Zhang Z, Yu Z M, and Wang X 2022 *Phys. Rev. B* **105** 134303
[47] Liu Q B, Wang Z, and Fu H H 2021 *Phys. Rev. B* **103** L161303
[48] Liu P F, Li J, Tu X H, Li H, Zhang J, Zhang P, Gao Q, and Wang B T 2021 *Phys. Rev. B* **103** 094306
[49] Zhang T, Takahashi R, Fang C, and Murakami S 2020 *Phys. Rev. B* **102** 125148
[50] Wang R, Xia B W, Chen Z J, Zheng B B, Zhao Y J, and Xu H 2020 *Phys. Rev. Lett.* **124** 105303
[51] Huang Z, Chen Z, Zheng B, and Xu H 2020 *npj Comput. Mater.* **6** 87
[52] Xia B W, Wang R, Chen Z J, Zhao Y J, and Xu H 2019 *Phys. Rev. Lett.* **123** 065501
[53] Liu J, Hou W, Wang E, Zhang S, Sun J T, and Meng S 2019 *Phys. Rev. B* **100** 081204
[54] Chen Z J, Wang R, Xia B W, Zheng B B, Jin Y J, Zhao Y J, and Xu H 2021 *Phys. Rev. Lett.* **126** 185301
[55] Jin Y, Wang R, and Xu H 2018 *Nano Lett.* **18** 7755
[56] Yang T, Gu Q, Wang P, Wu Z, and Zhang Z 2022 *Appl. Phys. Lett.* **121** 053102
[57] Zhang T T, Miao H, Wang Q, Lin J Q, Cao Y, Fabbris G, Said A H, Liu X, Lei H C, Fang Z, Weng H M, and Dean M P M 2019 *Phys. Rev. Lett.* **123** 245302
[58] Ding G, Sun T, Surucu G, Surucu O, Gencer A, and Wang X 2022 *Phys. Chem. Chem. Phys.* **24** 17210
[59] Wang J, Yuan H, Yu Z M, Zhang Z, and Wang X 2021 *Phys. Rev. Mater.* **5** 124203
[60] Li J, Xie Q, Liu J, Li R, Liu M, Wang L, Li D, Li Y, and Chen X Q 2020 *Phys. Rev. B* **101** 024301
[61] Liu G, Jin Y, Chen Z, and Xu H 2021 *Phys. Rev. B* **104** 024304
[62] Liu Q B, Fu H H, Xu G, Yu R, and Wu R 2019 *J. Phys. Chem. Lett.* **10** 4045
[63] Jin Y J, Chen Z J, Xia B W, Zhao Y J, Wang R, and Xu H 2018 *Phys. Rev. B* **98** 220103
[64] Wang R Y, Chen Z J, Huang Z Q, Xia B W, and Xu H 2021 *Phys. Rev. Mater.* **5** 084202
[65] Zheng B B, Xia B W, Wang R, Chen Z J, Zhao J Z, Zhao Y J, and Xu H 2020 *Phys. Rev. B* **101** 100303
[66] Zhou F, Zhang Z, Chen H, Kuang M, Yang T, and Wang X 2021 *Phys. Rev. B* **104** 174108
[67] Peng B, Hu Y, Murakami S, Zhang T, and Monserrat B 2020 *Sci. Adv.* **6** eabd1618
[68] Li J, Wang L, Liu J, Li R, Zhang Z, and Chen X Q 2020 *Phys. Rev. B* **101** 081403
[69] Deng W, Lu J, Li F, Huang X, Yan M, Ma J, and Liu Z 2019 *Nat. Commun.* **10** 1769
[70] Peng B, Murakami S, Monserrat B, and Zhang T 2021 *npj Comput. Mater.* **7** 195
[71] Chen Z J, Xie Z J, Jin Y J, Liu G, and Xu H 2022 *Phys. Rev. Mater.* **6** 034202
[72] Wang X, Zhou F, Yang T, Kuang M, Yu Z M, and Zhang G 2021 *Phys. Rev. B* **104** L041104
[73] Wang J, Yuan H, Liu Y, Zhou F, Wang X, and Zhang G 2022 *Phys. Chem. Chem. Phys.* **24** 2752
[74] Liu Q B, Wang Z Q, and Fu H H 2021 *Phys. Rev. B* **104** L041405
[75] Xie C, Yuan H, Liu Y, and Wang X 2022 *Phys. Rev. B* **105** 054307
[76] Xie C, Yuan H, Liu Y, Wang X, and Zhang G 2021 *Phys. Rev. B* **104** 134303
[77] Posey V A, Turkel S, Rezaee M *et al.* 2024 *Nature* **625** 483
[78] Mathur N D, Grosche F M, Julian S R *et al.* 1998 *Nature* **394** 39
[79] Gegenwart P, Si Q M, and Steglich F 2008 *Nat. Phys.* **4** 186
[80] Yazdani A, da Silva Neto E H, and Aynajian P 2016 *Annu. Rev. Condens. Matter Phys.* **7** 11
[81] Löhneysen H V, Rosch A, Vojta M, and Wölfle P 2007 *Rev. Mod. Phys.* **79** 1015
[82] Stewart G R 1984 *Rev. Mod. Phys.* **56** 755
[83] Jiao L, Howard S, Ran S, Wang Z Y, Rodriguez J O, Sigrist M, Wang Z Q, Butch N P, and Madhavan V 2020 *Nature* **579** 523
[84] Kresse G and Furthmüller J 1996 *Phys. Rev. B* **54** 11169
[85] Kresse G and Furthmüller J 1996 *Comput. Mater. Sci.* **6** 15
[86] Eriksson F, Fransson E, and Erhart P 2019 *Adv. Theory Simul.* **2** 1800184
[87] Wu Q, Zhang S, Song H F, Troyer M, and Soluyanov A A 2018 *Phys. Chem. Commun.* **224** 405
[88] Lopez Sancho M P, Lopez Sancho J M, Sancho J M L, and Rubio J 1985 *J. Phys. F* **15** 851